Ocean Sci. Discuss., 9, 2793–2815, 2012
www.ocean-sci-discuss.net/9/2793/2012/
doi:10.5194/osd-9-2793-2012

Ocean Science Discussions

Variability in the air–sea interaction patterns and time-scales within the Southeastern Bay of Biscay, as observed by HF radar data

A. Fontán[1], **G. Esnaola**[1], **J. Sáenz**[2], **and M. González**[1]

[1]AZTI-Tecnalia, Marine Research Division. Herrera Kaia, Portualdea, z/g, 20110 Pasaia, Spain
[2]Department of Applied Physics II, Fac. of Science and Technology, University of the Basque Country UPV/EHU, Sarriena Auzoa z/g, 48940 Leioa, Spain

Received: 2 July 2012 – Accepted: 16 August 2012 – Published: 31 August 2012

Correspondence to: A. Fontán (afontan@azti.es)

Published by Copernicus Publications on behalf of the European Geosciences Union.

Abstract

Two high frequency (HF) radar stations were installed on the Southeastern Bay of Biscay in 2009, providing high spatial and temporal resolution and large spatial coverage currents for the first time in the area. This has enabled to determine quantitatively the air–sea interaction patterns and time-scales for the period 2009–2010. The analysis was conducted by using the Barnett-Preisendorfer approach to canonical correlation analysis (CCA) of reanalysis surface winds and HF radar-derived currents. The results reveal that the CCA yields two canonical patterns. The first wind-current interaction pattern corresponds to the classical Ekman drift at sea surface, whilst the second describes an anticyclonic/cyclonic surface circulation. The results obtained demonstrate that the local winds play an important role in driving the upper water circulation. The wind-current interaction time-scales are mainly related to diurnal breezes and synoptic variability. In particular, the breezes force diurnal currents in the continental shelf and slope of the Southeastern Bay. It is concluded that the breezes may force diurnal currents over considerably wider areas than that covered by the HF radar, considering that the northern and southern continental shelves of the Bay exhibit stronger diurnal than annual wind amplitudes.

1 Introduction

The Bay of Biscay, located in the Eastern North Atlantic Ocean, is characterised by its complex submarine topography. This consists of an abyssal plain with water depths of around 4 500 m. The continental slope, formed by the Armorican, the Aquitaine and the Cantabrian slopes, is the transition between the deep sea and the continental shelf. This is very steep and fractured by numerous canyons. The continental shelf (water depths of less than 200 m) is wider in the northern part, whilst the southern part (Cantabrian shelf) is extremely narrow with a mean width between 30 and 40 km. The study area, Southeastern Bay of Biscay, is located in the innermost part of the

OSD
9, 2793–2815, 2012

Bay, where the orientation of the coast changes from east-west to north-south (Fig. 1). Here, the continental shelf is the narrowest ranging from 7 to 20 km wide (Pascual et al., 2004; Lavín et al., 2006).

The atmospheric circulation over the Bay is characterised by prevailing winds from the west to south-west. However, the winds are not spatially homogeneous and vary seasonally. In winter, the wind comes from the southwest and from the west–northwest in summer (OSPAR, 2000). In particular, within the Southeastern Bay, the dominant winds are from the southwest in winter and autumn, whereas northwesterly winds are the most frequent direction in spring and summer.

The surface water circulation over the region is mainly forced by the wind and partially constrained by the bathymetry. As such, the surface flow over the abyssal plain is eastward in winter, whereas it is to the south in summer in agreement with the seasonal wind-driven Ekman drift (Van Aken, 2002; Charria et al., 2012). Over the continental slope, the surface flow is derived from wind forcing and density field. The slope current is markedly seasonal in relation to the seasonal wind regimen in the Bay. In winter, the prevailing winds reinforce the slope current, flowing eastward along the Cantabrian slope. In summer, this current appears to be westward or absent with the prevalence of the southward wind stress (Pingree and Le Cann, 1990; Van Aken, 2002). Over the continental shelf, the surface currents are the result of the combined effect of the wind, buoyancy and tides. In the southern part of the Bay (south of 45° N), the tidal currents are relatively weak as the strength of the tidal currents is proportional to the shelf width (Koutsikopoulos and Le Cann, 1996). Smaller river runoff and a much narrower shelf off the Southern Bay make buoyant plumes much less persistent than those over the Armorican shelf. As a result, the surface currents are predominantly wind-induced in the southeastern shelf (Ibáñez, 1979; González et al., 2004).

Overall, in the Southeastern Bay of Biscay, surface water circulation is primarily driven by the wind forcing at the coast (Fontán et al., 2009, 2012) and the continental shelf (Ibañez, 1979; Álvarez-Salgado et al., 2006; González et al., 2006). On the Cantabrian continental slope, the surface circulation appears to be related to the

OSD
9, 2793–2815, 2012

density field and wind forcing. Recently, Herbert et al. (2011) concluded that the slope surface currents are partially driven by wind forcing at daily time-scales, as the local wind tends to favour or prevent the extension of the geostrophic current. It has to be stressed, however, that most of the research undertaken on the surface circulation, in the southeastern coastal and continental shelf areas together with that attempted in the continental slope (Caballero et al., 2008; González et al., 2008; Abascal et al., 2009; Rubio et al., 2012), has been focused on short-term datasets and fixed locations or model simulations.

Recently, the Directorate of Emergency Attention and Meteorology (Basque Government) has established an Operational Oceanography regional system in the area. At the beginning, the data acquisition system was formed by 6 coastal stations and 2 oceanic buoys, which provide oceanographic and meteorological information at fixed locations. In 2009, the system was complemented with the installation of a high frequency (HF) radar array. This has improved to a great extent the data acquisition system, providing measurements of marine currents with high temporal and spatial resolutions and large spatial coverage for the first time in the area. The present investigation, motivated by the availability of those observations, aims to explore and determine quantitatively the air–sea interaction patterns and time-scales within the Southeastern Bay of Biscay for the period 2009–2010. This has been accomplished by applying the Barnett and Preisendorfer (1987) approach to Canonical Correlation Analysis (CCA) of wind and current fields with high spatial and temporal resolutions. For this purpose, the data and the analytical procedures adopted are described in Sect. 2. Section 3 presents the wind variability and its influence on surface water circulation. The wind-current interaction patterns and time-scales are presented and discussed in Sect. 4. Finally, the main conclusions and future perspectives are given in Sect. 5.

OSD
9, 2793–2815, 2012

2 Data and methods

The data used in this study cover a 2-yr period (2009–2010) of hourly marine currents derived from the HF radar system. Two HF radar stations were installed in the Southeastern Bay of Biscay (see Fig. 1) and are operational since 2009. The stations are equipped with CODAR SeaSonde systems, working in the 4.5 MHz frequency band with a 40 kHz bandwidth. The antennae cover a 150 km range with a 5 km radial and 5° angular resolutions. The radial velocities were 3-h moving averaged and, hourly total current vectors were obtained from these radial velocities by a least squares approach with an interpolation radius of 20 km. Finally, hourly currents were derived over a regular mesh with a 5 km horizontal resolution. Standard quality control procedures were applied to radial and total velocities (see Rubio et al. (2011), for a detailed description). The HF radar currents were validated by Rubio et al. (2011); these authors concluded that the HF radar currents agree well with in situ measurements in the area.

The wind components at 10 m a.s.l. of the Climate Forecast System Reanalysis (CFSR), provided by the National Centres for Environmental Prediction (NCEP), were also used in this study (Saha et al., 2010). The wind dataset covers the period 1979–2010 and the spatial and temporal resolutions are of 0.312° and 1 h, respectively. These data were utilised to describe the wind variability and the air–sea interaction patterns over the area. Xue et al. (2011) validated the surface winds from the CFSR and concluded that they generally agree well with the observations over the region.

CCA of surface current and wind fields, for the period 2009–2010, was used to describe the wind-current interaction patterns along the Southeastern Bay of Biscay. This analysis identifies new basis vectors for two sets of variables such that the correlation between the projections of the variables onto these basis vectors are mutually maximised. In the present investigation, the Barnett and Preisendorfer (1987) approach to CCA was applied, which involves the application of an Empirical Orthogonal Function (EOF) analysis to the data prior to a classical CCA. This analysis presents advantages with respect to the classical CCA: the reduction of the dimensionality of the problem

OSD
9, 2793–2815, 2012

and of the noise of the original datasets and the use of uncorrelated data series. The HF radar grid points with more than 50 % data coverage were selected for the analysis (Fig. 1). In order to eliminate the effects of unwanted high frequency non-wind-induced motions prior to the EOF computation, a low-pass filter specially designed to supress inertial and semidiurnal tidal components (with a cut-off of 20 h and 137 points) was applied to the wind and current datasets (Thompson, 1983). This filter was used separately in each continuous data segment as the HF radar-derived currents contain data gaps. This latter implies the use of the Lomb-Scargle method to compute the power spectrum of unevenly spaced data (Press et al., 1992). Spectra were determined for each HF radar grid point and were then averaged in order to increase the number of degrees of freedom of the spectral estimates. Figure 2 shows that the semidiurnal tidal components (S_2 and M_2) and the inertial motions (T_i) have been appropriately eliminated from currents by applying the digital filter. Conversely, the wind-induced currents due to diurnal breezes (S_1) have been preserved in the low-pass filtered currents as shown in Fig. 2. Low-pass filtering (with a cut-off period of 20 h) of the CFSR winds was also performed to remove high-frequency signals.

All the data values were weighted by the square root of cosine of latitude prior to the EOF computation, to account for the latitudinal distortion in the case of a regular latitude-longitude grid. The EOF analysis was then applied for compressing the variability in both current and wind datasets. This was performed on both vector components by computing the eigenvalues and eigenvectors of their joint covariance matrix. This provides a compact description of temporal and spatial variability of datasets in terms of orthogonal functions, which are linear combinations of original variables. The new variables are called principal components (PCs) and are chosen to represent the maximum possible fraction of the variability in the original datasets (Wilks, 2006). The truncation criterion of the principal components was based on North's rule of thumb (North et al., 1982) and a Monte Carlo test on the congruence coefficients of the EOFs obtained from 5000 random subsamples and the whole sample (Cheng et al., 1995). Afterwards, the optimum number of PCs retained for CCA was selected

OSD
9, 2793–2815, 2012

by a cross-validation method (Feddersen, 2003; Feddersen and Andersen, 2005). In this procedure, the available data are repeatedly divided into validation and verification subsets in each time step. For each time, the CCA model is constructed based on data series that do not include values for that time. The neighbouring values are also excluded since the data are autocorrelated. Then the model is tested on the skipped observations, yielding predictive skill scores. Once the optimal number of PCs that maximise the performance of the CCA model was determined, the statistical significance of the canonical correlation coefficients was tested by means of a Monte Carlo approach. The time series were randomly resampled 5000 times, taking into consideration serial correlation, to obtain a statistical distribution of the canonical correlations that happen by chance in those samples (Feddersen, 2003; Feddersen and Andersen, 2005). Finally, the sensitivity of the results to the spatial scales selected for the winds was also tested by repeating the analysis for two domains (D1 and D2 in Fig. 1).

3 Atmospheric variability from reanalysis winds and its influence on surface circulation

The climatological winds, over the study area, vary spatially and at seasonal scales. The winds also vary at diurnal time-scales, due to the so-called land and sea breezes. This is one of the most prominent mesoscale phenomenon in coastal locations around the world (Kumar et al., 1986). These are classified as mesoscale according to the horizontal coverage and duration, with spatial scales between 20 and 200 km. Therefore, it is expected that the land and sea breezes may affect surface water circulation at such distances (20 to 200 km) from the coastal areas.

To explore the influence of winds on surface circulation, the diurnal and annual amplitudes have been extracted from CFSR surface winds for the period 1979–2010 (Fig. 3). It can be seen that the breezes increase towards the coast, with larger amplitudes in the coastal and continental shelf areas (Fig. 3a and b). The diurnal component exceeds annual component (the ratio is above 1) partially at the French continental shelf

OSD
9, 2793–2815, 2012

and at the Cantabrian continental shelf and slope (Fig. 3c). The diurnal breezes also vary seasonally, being stronger in spring and summer (Fig. 3b) than in autumn and winter (Fig. 3a). Apart from the well-known influence of the breezes in the coastal circulation over the Southeastern Bay of Biscay (Fontán et al., 2009, 2012), they appear to affect the surface water circulation mainly in the continental shelf, and to a lesser extent in the continental slope. The diurnal amplitudes extracted from HF radar observations (Fig. 3d) show that the diurnal currents are stronger in the continental shelf and decrease offshore according to the distribution of diurnal breezes (Fig. 3a–c). This is also consistent with the results of the spectral analysis performed on HF radar currents (Fig. 2): well-defined and significant peaks can be observed centred on diurnal period for both zonal and meridional currents. These diurnal currents are not primarily forced by astronomical tides, but rather, arise from diurnal breezes. In fact, diurnal tides and currents of astronomical origin are very weak in the Bay of Biscay (Le Cann, 1990). This is consistent with the results of several investigators (Hyder et al., 2002; Mihanović et al., 2009; Zaytsev et al., 2010; among others), who concluded that the breezes induce surface-intensified diurnal variability in water circulation.

These results show that the breezes induce diurnal water motions in the area. In addition, the diurnal winds are stronger in the summertime period and may generate stronger diurnal currents in the area. Finally, these findings indicate that the land and sea breezes are probably affecting surface water circulation over wider areas (such as the Cantabrian and Armorican continental shelves) than that covered by the HF radar system (Fig. 3c). In the next section, the wind-current interaction patterns and time-scales are explored and determined quantitatively by applying the CCA in the EOF space to wind and current datasets for the period 2009–2010.

4 Air–sea interaction patterns and time-scales

The Barnett and Preisendonfer (1987) approach to CCA was applied at the two different spatial scales (D1 and D2 in Fig. 1). Firstly, the number of predictors (i.e. winds) and

OSD
9, 2793–2815, 2012

predictands (i.e. currents) was prefiltered by applying the EOF analysis. This permitted to compress the variability and to avoid internal correlations in both fields. As above-mentioned, the optimal number of retained modes was determined by the North's rule of thumb (North et al., 1982) and a Monte Carlo test on the congruence coefficients. For the currents, the 12 leading EOFs are non-degenerated (94 % of current variance). For the wind, the truncation criterion was set to 14 at D1 and D2 spatial domains, which accounted for 98–99 % of the wind variability. This is consistent with the results obtained from the Monte Carlo test. This was performed on the congruence coefficients of the EOFs obtained by 5000 random subsamples with those obtained with the whole sample (not shown). It is worth noting that the time series used in the EOF analysis contain serial correlation and consequently, a higher number of EOFs is expected to be retained. As a first order approximation, the serial correlation was not considered in the Monte Carlo test, overestimating the number of EOFs retained. Subsequently, the maximum number of EOFs to be retained in the CCA analysis was estimated by a cross-validation approach (Feddersen, 2003; Feddersen and Andersen, 2005), taking into account the autocorrelation of the series. This enabled to avoid the overfitting in the CCA computations. To this end, the performance of the CCA model was tested by analysing all the combinations based on the 12 leading PCs for currents and the 14 leading PCs for winds at the two spatial scales (D1 and D2). As mentioned in Sect. 2, the cross-validation approach was applied by withholding the serially correlated time interval from every dataset in each time step and then predicting it, based on the remaining data. This process was repeated for each time step. Finally, the performance of the CCA models was evaluated by calculating the correlation coefficient (Fig. 4a), the bias (Fig. 4b) and the root mean square error (Fig. 4c) between the predicted and the withheld data. The abscissa axis in Fig. 4 represents the number of wind EOFs retained to design the CCA model, whilst the ordinate axis corresponds to the number of current EOFs used. It can be seen that increasing the number of wind EOFs above 2, the correlation coefficient decreases and the RMSE increases. The increase of the number of current EOFs above 6 does not significantly improve the skill scores.

OSD
9, 2793–2815, 2012

Therefore, it can be concluded that the best predictive skills are obtained when the 6 and the 2 leading PCs of currents and winds, respectively, are retained at the D1 domain. The results obtained are similar at the D2 domain (not shown).

Afterwards, CCA on the 2 leading PCs of wind and the 6 leading PCs of currents (87 % and 86 % of the current and wind variance, respectively) was performed at the two spatial domains. The canonical correlation coefficients for mode 1 (2) are 0.84 (0.70) and 0.79 (0.57) (statistically significant above the 99.99 % confidence level against the null hypothesis that the series are uncorrelated) for the D1 and D2 domains, respectively. The largest canonical correlations are obtained for the D1 domain. Taking into consideration that the increase of the spatial domain does not improve the canonical correlations, only the D1 spatial domain will be considered herein. The CCA model shows enhanced results over shorter spatial scales (D1 domain), which means that the currents are mainly forced by the local wind effects in the study area. Additionally, the wind and currents show the strongest correlation at zero lag, which denotes that the currents respond almost instantaneously to the wind forcing (note that the currents have been 3-h moving averaged during data pre-processing).

The spatial patterns corresponding to each CCA mode have been scaled in the units of the original fields. To this end, homogeneous regression maps have been constructed (i.e. the regression between each CCA temporal expansion coefficient and its corresponding original field) for both current and wind fields. These regression maps between the original data and the temporal coefficients corresponding to each CCA mode are shown in Fig. 5. The first canonical mode exhibits a correlation, between the wind and current derived canonical variables, of 0.84. Each canonical variable explains 43.7 % of the wind and 25.8 % of the current variance. Its corresponding spatial pattern shows that the currents flow at an angle with the driving wind (Fig. 5a). This is consistent with the wind-induced Ekman drift at sea surface. As such, the surface currents are found to be to the right of the wind forcing. This is in agreement with the results obtained by several authors in other areas, based on HF radar measurements. For instance, Son et al. (2007) also described a predominant Ekman response of subtidal

OSD
9, 2793–2815, 2012

flow in South Korea. Yoshikawa et al. (2007) identified a current profile corresponding to the Ekman spiral in the Tsushima Strait (based on observations from current profilers and HF radar) by using EOF analysis. Yoshikawa and Masuda (2009) also reported a larger deflection angle of the wind-induced flow in summer than in winter due to changes in the momentum penetration by seasonal stratification change. The wind impulse response and transfer functions have been widely discussed with HF radar currents in California and interpreted with Ekman theory by Kim et al. (2009, 2010). Zhao et al. (2011) also attributed the subtidal flow to Ekman wind-induced dynamics in waters of Qingdao (China).

With regard to the second canonical mode, the canonical correlation is lower (0.70) than that obtained for the first canonical mode (0.84). However, the variance explained is similar to that of the first canonical mode: 42.3 % of the wind and 26.0 % of the current. This spatial pattern shows an anticyclonic surface water circulation for positive phases of the canonical correlation coefficient (anomalies are reversed for negative phases). This appears to be wind-driven, excluding the northwesternmost area where the currents flow in the opposite direction to the wind forcing. In order to confirm that this second CCA mode is not an artefact, we have repeated the analysis for two independent subsets of current data (not shown). The first subset corresponds to grid points in the continental shelf (depth < 200 m), whilst the second subset grid points are distributed in the continental slope (depth > 200 m). The results obtained indicate that both subsets yield the same canonical patterns, so that the second CCA mode is robust. It is worth noting now that the radar observations, at 4.5 MHz frequency, correspond to vertically averaged currents within the upper 2–3 m (Rubio et al., 2011). Consequently, HF radar-derived measurements may integrate other processes with the first 2–3 m of the water column apart from the wind-induced flows. However, the investigation of other possible mechanisms for driving the anticyclonic/cyclonic surface circulation, in the second canonical mode, is out of the scope of the present investigation.

Finally, the normalised periodograms of the canonical variables have been calculated in order to determine the wind-current interaction time-scales (Fig. 6). Well-defined

OSD
9, 2793–2815, 2012

and significant peaks (99 % confidence level) can be observed, centred on the diurnal (S_1) period for both canonical series. This finding confirms that the diurnal breezes generate currents not only at coastal locations (Fontán et al., 2012) but also at the continental shelf and slope as observed in Fig. 3. Several additional, but less resolved, simultaneous spectral peaks on both wind and current derived canonical variables can be seen at synoptic time-scales. No other spectral peaks can be observed, mainly due to the limited number of observations (only 2 yr with less than 50 % data coverage). Further investigation is needed to explore wind-current interaction time-scales based on long-term data series.

5 Concluding remarks and future perspectives

The conclusions obtained from the diagnostic of wind-induced currents can be summarised as follows. The air–sea interaction patterns obtained reveal that the currents respond almost instantaneously to wind forcing at hourly resolution. The local winds are the main driving force of the upper currents at the Southeastern Bay of Biscay. The Barnett-Preisendorfer approach to CCA yields two canonical patterns, which explain each of about 43 % and 26 % of the wind and current variance, respectively. The first wind-current interaction pattern corresponds to the classical Ekman drift at sea surface, with current deflected a clockwise angle with respect to the wind forcing. Conversely, the second canonical pattern reveals an anticyclonic water movement. Although this appears to be partially wind-driven, other driving mechanisms may contribute to it. Further research is required to identify other possible driving dynamics of the upper water circulation in the Bay, in order to fully substantiate this mode. The air–sea interaction time-scales are related to diurnal periods, revealing that the breezes force diurnal currents at the continental shelf and slope. Synoptic wind circulation also affects surface water circulation over the area. The extension of the area, where the amplitude of diurnal cycle is larger than that of the seasonal cycle (Fig. 3), indicates that this process

OSD
9, 2793–2815, 2012

is probably affecting surface water circulation over considerably wider areas than that covered by the HF radar system.

In recent years, there is an increasing literature about statistical models based on HF radar currents. For instance, Zelenke (2005) developed a linear statistical model for short term prediction of surface circulation based on wind forecasts and HF radar currents. O'Donnell et al. (2005) evaluated forecasting algorithms based on cross-covariance functions between surface currents and winds. Recently, Frolov et al. (2012) proposed an empirical method for predicting surface currents based on short history of HF radar observations and predicted winds by using EOF analysis. In the present case, the results obtained suggest that the EOF-CCA approach can also be adequate to undertake a statistical prediction model related to surface winds and HF radar observations. The prediction of surface currents can be undertaken based on accurate meteorological predictions at short time-scales. This statistical model appears to be easier to implement and maintain than the classical numerical modelling. In addition, the performance and accuracy of the statistical modelling can be easily improved by increasing the number of observations. Finally, accurate and rapid predictions of surface currents will provide to decision-makers valuable information for oil spill detection, search and rescue, marine safety, offshore operations and risk assessment, among others. Future studies of the authors will evaluate the feasibility of such a model.

Acknowledgements. The authors acknowledge financial support from the ETORTEK Strategic Research Programme (Department of Industry, Trade and Tourism and Department of Transport and Civil Works of the Basque Government) through the ITSASEUS II project. We thank Qualitas Remos for the work performed on HF radar data processing. We also thank L. Solabarrieta for her enthusiasm and interest on HF radar measurements. Jon Sáenz would like to thank financial support from projects CGL2008-03321 (Spanish National R+D+I Programme) and CTPIO-03 PYNATEO (Basque Government). He also thanks funding provided by the University of the Basque Country (UFI 11/55 and GIU 11/01). The wind data for this study are from the Research Data Archive (RDA), which is maintained by the Computational and Information Systems Laboratory (CISL) at the National Center for Atmospheric Research (NCAR). NCAR is sponsored by the National Science Foundation (NSF). The original data are available from

OSD
9, 2793–2815, 2012

the RDA (http://dss.ucar.edu) in dataset number ds093.1. G. Esnaola is being supported by a research grant from the Fundación Centros Tecnológicos, Iñaki Goenaga. This is contribution number XXX, of the Marine Research Division of AZTI-Tecnalia.

References

Abascal, A. J., Castanedo, S., Méndez, F. J., Medina, R., and Losada, I. J.: Calibration of a lagrangian transport model using drifting buoys deployed during the Prestige oil spill, J. Coast. Res., 25, 80–90, 2009.

Álvarez-Salgado, X. A., Herrera, J. L., Gago, J., Otero, P., Soriano, J. A., Pola, C. G., and García-Soto, C.: Influence of the oceanographic conditions during spring 2003 on the transport of the Prestige tanker fuel oil to the Galician coast, Mar. Pollut. Bull., 53, 239–249, 2006.

Barnett, T. P. and Preisendorfer, R. W.: Origins and levels of monthly and seasonal forecast skill for United States surface air temperatures determined by canonical correlation analysis, Mon. Weather Rev., 115, 1825–1850, 1987.

Caballero, A., Espino, M., Sagarminaga, Y., Ferrer, L., Uriarte, A., and González, M.: Simulating the migration of drifters deployed in the Bay of Biscay, during the Prestige crisis, Mar. Pollut. Bull., 56, 475–482, 2008.

Charria, G., Lazure, P., Le Cann, B., Serpette, A., Reverdin, G., Louazel, S., Batifoulier, F., Dumas, F., Pichon, A., and Morel, Y.: Surface layer circulation derived from subsurface Lagrangian drifters in the Bay of Biscay, J. Mar. Syst., in press., 2012.

Cheng X., Nitsche, G., and Wallace, J. M.: Robustness of low-frequency circulation patterns derived from EOF and rotated EOF analyses, J. Climate, 8, 1709–1713, 1995.

Feddersen, H.: Predictability of seasonal precipitation in the Nordic region, Tellus A, 55, 385–400, 2003.

Feddersen, H. and Andersen, U.: A method for statistical downscaling of seasonal ensemble predictions, Tellus A, 57, 398–408, 2005.

Fontán, A., González, M., Wells, N., Collins, M., Mader, J., Ferrer, L., Esnaola, G., and Uriarte, A.: Tidal and wind-induced circulation within the southeastern limit of the Bay of Biscay: Pasaia Bay, Basque coast, Cont. Shelf Res., 29, 998–1007, 2009.

OSD

9, 2793–2815, 2012

Fontán, A., Sáenz, J., González, M., Rubio, A., Esnaola, G., Liria, P., Ganzedo, U., Hernández, C., and Collins, M.: Coastal water circulation response to radiational and gravitational tides within the Southeastern Bay of Biscay, J. Mar. Syst., in press., 2012.
Frolov, S., Paduan, J., Cook, M., and Bellingham, J.: Improved statistical prediction of surface currents based on historic HF-radar observations, Ocean Dynam., 62, 1111–1122, 2012.
González, M., Uriarte, A., Fontán, A., Mader, J., and Gyssels, P.: Marine dynamics, in: Oceanography and Marine Environment of the Basque Country, edited by: Borja, Á. and Collins, M., Elsevier Oceanography Series no. 70, Elsevier, Amsterdam, 133–157, 2004.
González, M., Uriarte, A., Pozo, R., and Collins, M.: The Prestige crisis: operational oceanography applied to oil recovery, by the Basque fishing fleet, Mar. Pollut. Bull., 53, 369–374, 2006.
González, M., Ferrer, L., Uriarte, A., and Urtizberea, A.: Operational oceanography system applied to the Prestige oil-spillage event, J. Mar. Syst., 72, 178–188, 2008.
Herbert, G., Ayoub, N., Marsaleix, P., and Lyard, F.: Signature of the coastal circulation variability in altimetric data in the Southern Bay of Biscay during winter and fall 2004, J. Mar. Syst., 88, 139–158, 2011.
Hyder, P., Simpson J. H., and Christopoulos S.: Sea-breeze forced diurnal surface currents in the Thermaikos Gulf, North-West Aegean, Cont. Shelf Res., 22, 585–601, 2002.
Ibáñez, M.: Hydrological studies and surface currents in the coastal area of the Bay of Biscay, Lurralde, 2, 37–75, 1979.
Kim, S. Y., Cornuelle, B. D., and Terrill, E. J.: Anisotropic response of surface currents to the wind in a coastal region, J. Phys. Oceanogr., 39, 1512–1533, doi:10.1175/2009JPO4013.1, 2009.
Kim, S. Y., Cornuelle, B. D., and Terrill, E. J.: Decomposing observations of high-frequency radar-derived surface currents by their forcing mechanisms: locally wind-driven surface currents, J. Geophys. Res., 115, C12046, doi:10.1029/2010JC006223, 2010.
Koutsikopoulos, C. and Le Cann, B.: Physical processes and hydrological structures related to the Bay of Biscay anchovy, Sci. Mar., 60, 9–19, 1996.
Kumar, A. R., Rao, M. P., and Murthy, J. S. R.: The effect of sea breeze on atmospheric stability as observed with acoustic sounder, Bound.-Lay. Meteorol., 35, 303–311, 1986.
Lavín, A., Valdes, L., Sánchez, F., Abaunza, P., Forest, A., Boucher, J., Lazure, P., and Jegou, A. M.: The Bay of Biscay: the encountering of the ocean and the shelf, in: The Sea, Vol.

OSD
9, 2793–2815, 2012

14B: The Global Coastal Ocean. Interdisciplinary Regional Studies and Syntheses, edited by: Robinson, A. R. and Brink, K., Harvard University Press, Cambridge, 933–1001, 2006.
Le Cann, B.: Barotropic tidal dynamics of the Bay of Biscay shelf: observations, numerical modelling and physical interpretation, Cont. Shelf Res., 10, 723–758, 1990.
Mihanović, H., Orlic, M., and Pasaric, Z.: Diurnal thermocline oscillations driven by tidal flow around an island in the Middle Adriatic, J. Mar. Syst., 78, 157–168, 2009.
North, G. R., Moeng, F. J., Bell, T. J., and Cahalan, R. F.: Sampling errors in the estimation of empirical orthogonal functions, Mon. Weather Rev., 110, 699–706, 1982.
O'Donnell, J., Ullman, D., Spaulding, M., Howlett, E., Fake, T., Hall, P., Tatsu, I., Edwards, C., Anderson, E., McClay, T., Kohut, J., Allen, A., Lester, S., and Lewandowski, M.: Integration of Coastal Ocean Dynamics Application Radar (CODAR) and Short-Term Prediction System(STPS) surface current estimates into the Search and Rescue Optimal Planning System (SAROPS), US Coast Guard Tech. Rep., USA, DTCG39-00-D-R00008/HSCG32-04-J-100052, 2005.
OSPAR: OSPAR Quality Status Report 2000, Region IV, Bay of Biscay and Iberian Coast, OSPAR Commission, London, 2000.
Pascual, A., Cearreta, A., Rodríguez-Lázaro, J., and Uriarte, A.: Geology and palaeoceanography, in: Oceanography and Marine Environment of the Basque Country, Elsevier Oceanography Series no. 70, edited by: Borja, Á. and Collins, M., Elsevier, Amsterdam, 53–73, 2004.
Press, W. H., Flannery, B. P., Teukolsky, S. A., and Vetterling, W. T.: Numerical Recipes in Fortran 77: The Art of Scientific Computing, Cambridge University Press, Cambridge, 1992.
Pingree, R. D. and Le Cann, B.: Structure, strength and seasonality of the slope currents in the Bay of Biscay region, J. Mar. Biol. Assoc. UK, 70, 857–885, 1990.
Rubio, A., Reverdin, G., Fontán, A., González, M., and Mader, J.: Mapping near-inertial variability in the SE Bay of Biscay from HF radar data and two offshore moored buoys, Geophys. Res. Lett., 38, 1–6, 2011.
Rubio, A., Fontán, A., Lazure, P., González, M., Valencia, V., Ferrer, L., Mader, J., and Hernández, C.: Seasonal to tidal variability of currents and temperature in waters of the continental slope, Southeastern Bay of Biscay, J. Mar. Syst., in press., 2012.
Saha, S., Moorthi, S., Pan, H.-L., Wu, X., Wang, J., Nadiga, S., Tripp, P., Kistler, R., Woollen, J., Behringer, D., Liu, H., Stokes, D., Grumbine, R., Gayno, G., Wang, J., Hou, Y.-T., Chuang, H.-Y., Juang, H.-M. H., Sela, J., Iredell, M., Treadon, R., Kleist, D., Van Delst, P., Keyser, D., Derber, J., Ek, M., Meng, J., Wei, H., Yang, R., Lord, S., Van Den Dool, H., Kumar, A., Wang,

OSD
9, 2793–2815, 2012

W., Long, C., Chelliah, M., Xue, Y., Huang, B., Schemm, J.-K., Ebisuzaki, W., Lin, R., Xie, P., Chen, M., Zhou, S., Higgins, W., Zou, C.-Z., Liu, Q., Chen, Y., Han, Y., Cucurull, L., Reynolds, R. W., Rutledge, G., and Goldberg, M.: The NCEP climate forecast system reanalysis, B. Am. Meteorol. Soc., 91, 1015–1057, 2010.

Son, Y.-T., Lee, S.-H., Kim, C.-S., Lee, J. C., and Lee, G.-H.: Surface current variability in the Keum River Estuary (South Korea) during summer 2002 as observed by high-frequency radar and coastal monitoring buoy, Cont. Shelf Res., 27, 43–63, 2007.

Thompson, R. O. R. Y.: Low-pass filters to suppress inertial and tidal frequencies, J. Phys. Oceanogr., 13, 1077–1083, 1983.

Van Aken, H. M.: Surface currents in the Bay of Biscay as observed with drifters between 1995 and 1999, Deep-Sea Res. Pt. I, 49, 1071–1086, 2002.

Wilks, D. S.: Statistical Methods in the Atmospheric Sciences, 2nd edn., International Geophysics Series, Vol. 59, Academic Press, New York, 2006.

Xue, Y., Huang, B., Hu, Z. Z., Kumar, A., Wen, C., Behringer, D., and Nadiga, S.: An assessment of oceanic variability in the NCEP climate forecast system reanalysis, Clim. Dynam., 37, 2511–2539, 2011.

Yoshikawa, Y., Matsuno, T., Marubayashi, K., and Fukudome, K.: A surface velocity spiral observed with ADCP and HF radar in the Tsushima strait, J. Geophys. Res., 112, C06022, doi:10.1029/2006JC003625, 2007.

Yoshikawa, Y. and Masuda, A.: Seasonal variations in the speed factor and deflection angle of the wind-driven surface flow in the Tsushima Strait, J. Geophys. Res., 114, C12022, doi:10.1029/2009JC005632, 2009.

Zaytsev, O., Rabinovich A. B., Thomson R. E., and Silverberg N.: Intense diurnal surface currents in the Bay of La Paz, Mexico, Cont. Shelf Res., 30, 608–619, 2010.

Zelenke, B. C.: An empirical statistical model relating winds and ocean surface currents: Implications for short-term current forecasts, M.S. thesis, Dept. of Oceanography, Oregon State University, Oregon, 94 pp., available at: http://hdl.handle.net/1957/2166, last access: 16 August 2012, 2005.

Zhao, J., Chen, X., Hu, W., Chen, J., and Guo, M.: Dynamics of surface currents over Qingdao coastal waters in August 2008, J. Geophys. Res., 116, C10020, doi:10.1029/2011JC006954, 2011.

OSD
9, 2793–2815, 2012

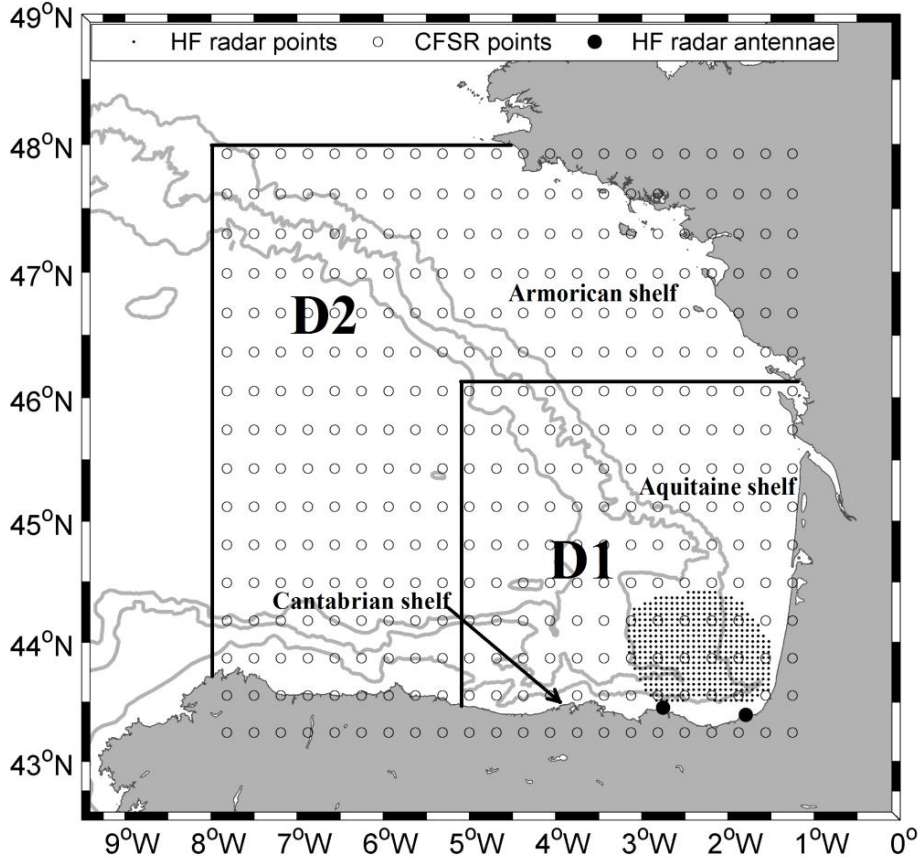

Fig. 1. Location of the study area showing the position of the HF radar points, with more than 50 % data coverage, CFSR grid points, HF radar antennae and the two considered spatial domains (D1 and D2). Bathymetric contours show the 200, 2000 and 4000 m isobaths.

OSD
9, 2793–2815, 2012

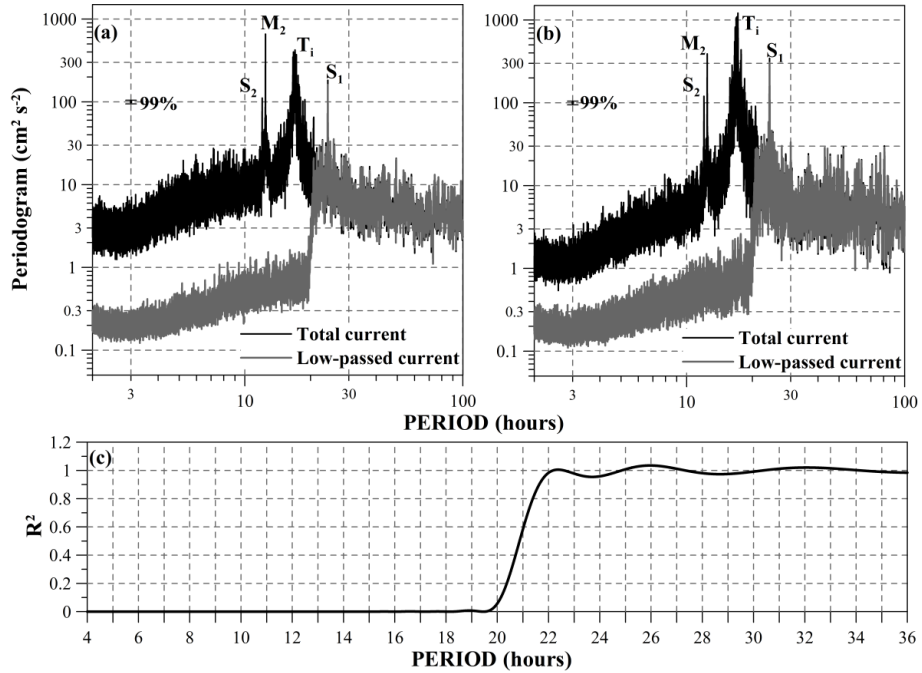

Fig. 2. Averaged Lomb-Scargle periodogram (99 % confidence level) for: **(a)** zonal and **(b)** meridional HF radar currents for the period 2009–2010. Spectra were computed on total and low-pass filtered currents. **(c)** Response factor (R) of the low-pass filter (with a cut-off of 20 h and 137 points). Note: S_2 is semidiurnal principal solar gravitational tide, M_2 is semidiurnal principal lunar gravitational tide, T_i is inertial motion and S_1 is wind-induced (breezes) diurnal component.

OSD
9, 2793–2815, 2012

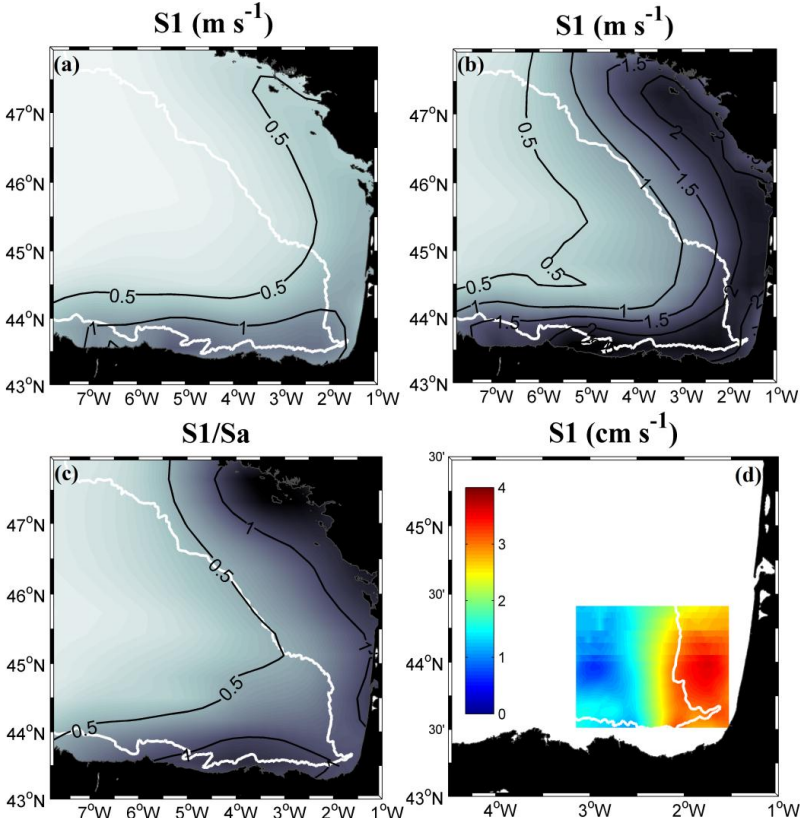

Fig. 3. The amplitude ($m\,s^{-1}$) of the diurnal (S1) harmonic of the surface wind speed from CFSR in: **(a)** wintertime (October–March) and **(b)** summertime (April to September) periods. **(c)** The ratio of the diurnal to the annual (Sa) components is also presented for the period 1979–2010. **(d)** The amplitude ($cm\,s^{-1}$) of the diurnal harmonic of the surface current speed derived from HF radar for the period 2009–2010. Bathymetric contour (solid white line) shows the 200 m isobath.

OSD
9, 2793–2815, 2012

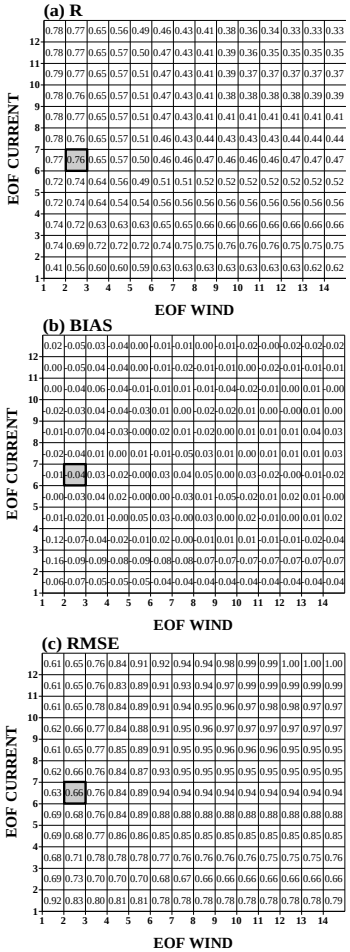

Fig. 4. Selection of the optimal CCA model at the D1 spatial domain by means of cross-validation. **(a)** Correlation coefficient (R), **(b)** bias and **(c)** root mean square error (RMSE).

OSD
9, 2793–2815, 2012

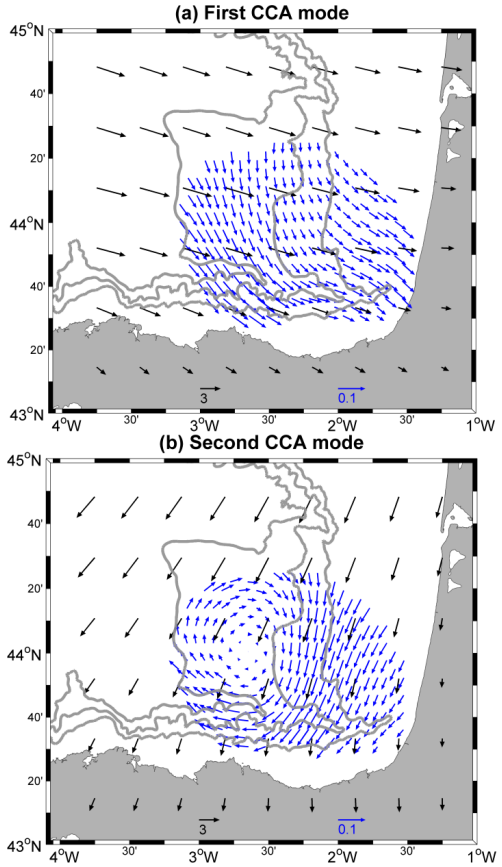

Fig. 5. Homogeneous regression maps of the **(a)** first and **(b)** second CCA modes for currents (blue) and wind (black) at the D1 domain. Bathymetric contours show the 200, 1000 and 2000 m isobaths.

OSD
9, 2793–2815, 2012

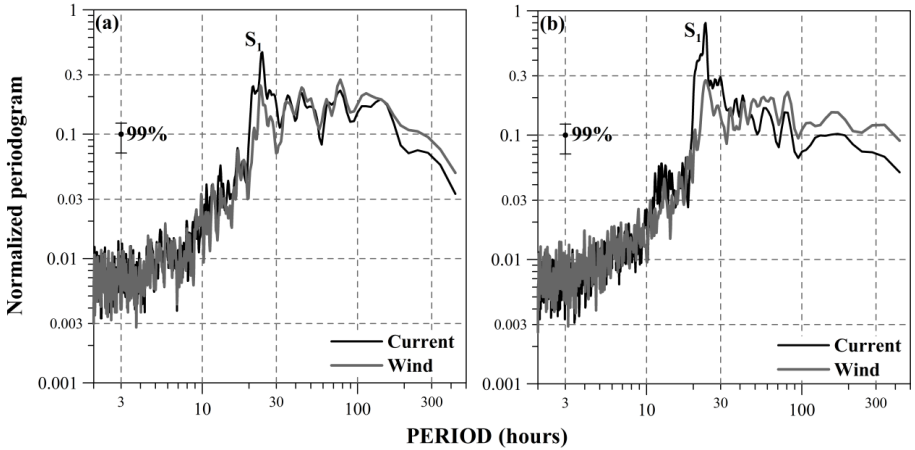

Fig. 6. Normalised Lomb-Scargle periodograms (99 % confidence level) for: **(a)** the first and **(b)** the second canonical variables of the wind and currents. Note: S_1 label corresponds to the diurnal wind component (breezes).

OSD
9, 2793–2815, 2012